Supporting Information

Competitive Nucleation Mechanism for $CsPbBr_3$ Perovskite Nanoplatelet Growth

Victor M. Burlakov[1,3], Yasser Hassan[2], Mohsen Danaie[4], Henry J. Snaith[2], and Alain Goriely[3]

[1]*Linacre College, University of Oxford, Oxford, OX1 3JA, UK*

[2]*Department of Physics, University of Oxford, Clarendon Laboratory, Parks Road, Oxford OX1 3PU, UK*

[3]*Mathematical Institute, Woodstock Road, Andrew Wiles Building, University of Oxford, Oxford, OX2 6GG, UK*

[4]*Diamond Light Source Ltd., electron Physical Science Imaging Centre (ePSIC), Harwell Science & Innovation Campus, Didcot, OX11 0DE.*

The effective ligand-ligand interaction energy

As it is illustrated by our simulations, the regime of nano-platelets growth is achieved in a relatively narrow range of the ligand-ligand interaction energies. The ligand contains a typically surface binding atomic group and a more or less extended molecular tail. In particular, the longer is the ligands' tail, the stronger is the ligand-ligand interaction, i.e., the higher is the corresponding interaction energy. In practice, the tail length cannot be fine-tuned due to the discreteness of the constituent molecular groups. Therefore, it could be more practical to use the mixture of ligands and fine-tune its composition to achieve the required effective ligand-ligand interaction energy. The analysis presented below illustrates the possibility of such an approach.

Formally we can represent a large enough surface cluster containing n_1 ligands of type '1' and n_2 ligands of type '2' as a 2-D mixed crystal, which in case of square symmetry (each ligand has four nearest neighbors) has the free energy

$$F_m = -E_{SL}\cdot\left(n_1+n_2\right) - 4\left(E_{11}n_1^2 + 2E_{12}n_1n_2 + E_{22}n_2^2\right)/\left(n_1+n_2\right) + \\ +k_BT\left(n_1\ln\left(\frac{n_1}{n_1+n_2}\right)+n_2\ln\left(\frac{n_2}{n_1+n_2}\right)\right) \qquad \text{(S1)}$$

where E_{SL} is ligand-surface binding energy, which is assumed to be the same for ligand 1 and 2, and E_{11} and E_{22} being corresponding ligand-ligand interaction energies. We want to illustrate that the ligand mixture in the cluster can be replaced with one type of ligands with an effective ligand-ligand pair interaction energy E_{LL}. The homogeneous crystal-free energy is

$$F_h = -n_L\left(E_{SL}+4E_{LL}\right) \qquad \text{(S2)}$$

where $n_L = n_1 + n_2$. We take the difference of Eqs (A1) and (A2) and equate it to '0.'

$$F_m - F_h = -\frac{4}{n_L}\left(E_{11}n_1^2 + 2E_{12}n_1n_2 + E_{22}n_2^2\right) + n_L\left(4E_{LL} + k_BT\frac{n_1}{n_L}\ln\left(\frac{n_1}{n_L}\right) + k_BT\left(\frac{n_2}{n_L}\right)\ln\left(\frac{n_2}{n_L}\right)\right) = 0 \quad \text{(S3)}$$

To simplify Eq. (A3) we assume that the ligands have the same surface binding group but different tail lengths; therefore, the ligand-ligand interaction is determined by the ligands with the shortest tail. Assuming that the shortest are the ligands of type '1' we can replace E_{12} with E_{11} and Eq. (A3) then reduces to

$$E_{LL} = E_{11} + \left(E_{22} - E_{11}\right)\left(\frac{n_2}{n_L}\right)^2 - \frac{1}{4}k_BT\left[\left(1-\frac{n_2}{n_L}\right)\ln\left(1-\frac{n_2}{n_L}\right) + \frac{n_2}{n_L}\ln\left(\frac{n_2}{n_L}\right)\right] \quad \text{(S4)}$$

This expression illustrates that a small variation in the concentration $\delta\left(n_2/n_L\right)$ of the ligands with longer tail hence with $E_{22} > E_{11}$ produces the small variation in the effective ligand-ligand interaction energy

$$\delta E_{LL} = \delta\left(\frac{n_2}{n_L}\right)\cdot\left[2\left(E_{22} - E_{11}\right) - \frac{1}{4}k_BT\ln\left(\frac{n_2}{n_L - n_2}\right)\right] \quad \text{(S5)}$$

thus, allowing fine-tuning of the latter.

Free energy of the critical cluster

Cluster formation caries an energy penalty associated with the transfer of free moving atoms or molecules (ligands) from solution to cluster. The change in the system's free energy related to the formation of atomic or ligand cluster of *N* units on the crystal surface can, therefore, be written as

$$\Delta F_A\left(N\right) = E_A\left(\varepsilon_{AA}, N\right) - Nk_BT\ln\left(n_A\right),\ \Delta F_L\left(N\right) = E_L\left(\varepsilon_{LL}, \varepsilon_{LA}, N\right) - Nk_BT\ln\left(n_L\right) \quad \text{(S6)}$$

where $E_A(\varepsilon_{AA}, N)$ and $E_L(\varepsilon_{LL}, \varepsilon_{LA}, N)$ are the total interaction energies within corresponding clusters (nuclei), ε_{AA}, ε_{LL} and ε_{LA} (all taken positive) are pairwise atom-atom, ligand-ligand, and atom-ligand interaction energies measured relative to atom/ligand energies in solution, n_A and n_L are volume concentrations of corresponding bare (unbound) species in solution and $k_B T$ is the system temperature in energy units. The interaction energies $E_A(\varepsilon_{AA}, N)$ and $E_L(\varepsilon_{LL}, N)$ are calculated as the sums of pairwise interaction energies ε_{AA}, ε_{LL} and ε_{LA}, assuming that atoms/ligands occupy cells in a square lattice and interact only with a maximum of four nearest neighbors inside the plane and with one neighbor beneath it. The cluster on the square lattice is formed such that it corresponds to the maximum interaction energy (lowest total energy), which corresponds to the maximum number of nearest neighbors (see Figure S1). It can be shown that the corresponding configuration is a square if $\sqrt{N}$ is an integer or a rectangle otherwise. Once the square cluster hits the facet edge (see the third rectangle from the end) it continues to grow as a rectangle stretching along that edge.

During crystal growth, the atoms are deposited on crystal facets, and their concentration in surrounding solution decreases. This decrease results in an increase of the critical nucleus size such that nucleation might not be possible on narrow crystal facets anymore - compare the panels a) and b) in Figure S2. This explains why the narrow facets can stop supporting the growth process even if they are not covered with ligands. The wider (4 u.c.) facets are still able to grow - see Figure S2c.

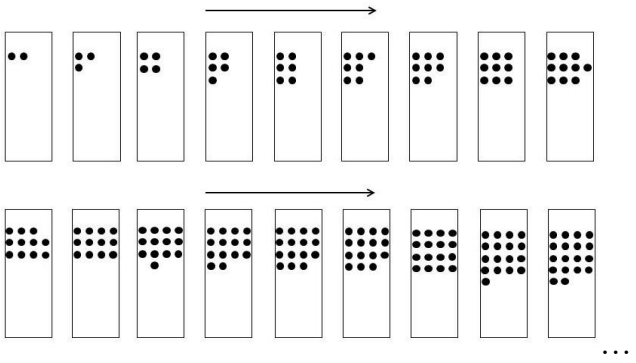

Figure S1. The lowest energy pathway for the nucleus formation (see text) on a square lattice. The rectangle depicts crystal facet, and the circles are atoms sequentially deposited on the face and placed in the lattice sites.

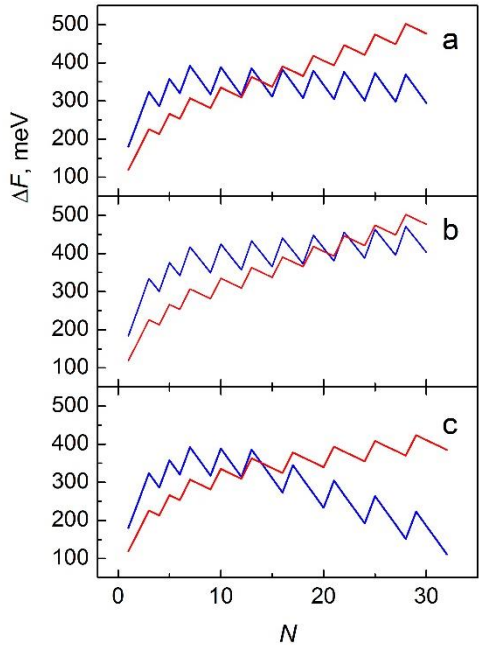

Figure S2. Excess free energies ΔF plotted versus cluster size N (given in unit cells) for different values of n_A: a) $n_A = 2.5 \cdot 10^{-4}$, b) and c) $n_A = 2.3 \cdot 10^{-4}$, and on crystal faces of different size: a) and b) 3x10, c) 4x8. The other parameters are $\varepsilon_{AA} = 109\,meV$, $\varepsilon_{LA} = 171\,meV$, $\varepsilon_{LL} = 66\,meV$, $n_L = 2.5 \cdot 10^{-4}$, $T = 134^o\,C$.

The spontaneous broadening of edge size distribution in nucleation-controlled crystal growth:

Nucleation controlled crystal growth is characterized by a relatively low probability of layer formation. For a better understanding of the properties of this growth, mode considers just a single crystal facet and derive the probability distribution $P(n, N_0)$ for this facet to accumulate a

certain number n of layers out of N_0 ($N_0 >> 1$) attempts (simulation steps). For simplicity, we assume that the growth rate or the probability p for a single layer to be deposited at each step is constant. As all deposition events are statistically independent, we may write for $P(n, N_0)$

$$P(n, N_0) = \frac{N_0!}{(N_0 - n)!n!} \cdot p^n \cdot (1-p)^{N_0 - n} \tag{S7}$$

This distribution gives the correct average value for the number of deposited layers

$$\langle n \rangle = \sum_{n=1}^{N_0} W(n, N_0) = p \cdot N_0,\ W(n, N_0) = n \cdot P(n, N_0) \tag{S8}$$

The term $W(n, N_0)$ under the sum in Equation (S8) has the meaning of the distribution of the deposited thickness, or, in other words, the distribution of the appropriate edge length measured in unit cells.

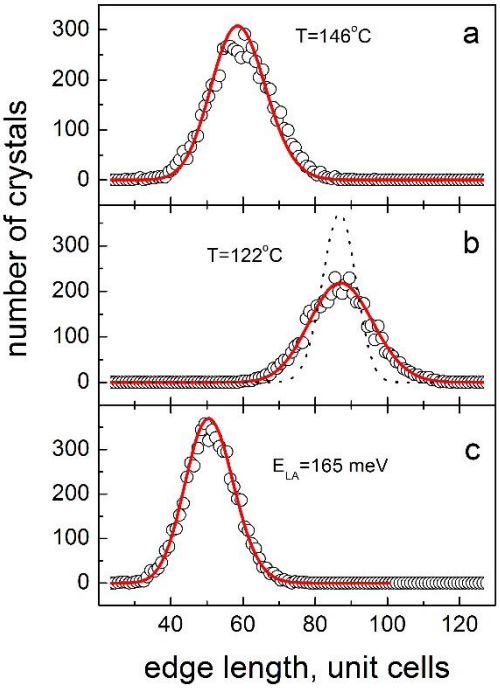

Figure S3. Edge distributions obtained in KMC simulations (symbols): a) the sum of all edges distributions from Fig. 3a, b) the sum of medium and long edges' distributions from Figure 3c, c) the sum of all distributions from Figure 4a. Red curves are the distributions $W(n, N_0)$ (see

Equation (S8)) for $p = 0.1$ and N_0 chosen to match corresponding peak positions. The dotted line in the panel b) is for $p = 0.75$.

We, therefore, can compare the edge length distributions from Figures 3 and 4 with $W(n, N_0)$. Choosing $p = 0.1$ and selecting N_0 such that the peak position of $W(n, N_0)$ coincides with that of the corresponding distribution obtained from KMC simulations, we achieve quite good agreement shown in Figure S3 using just a scaling along y-axes.

Worth noting that decreasing the probability *p* down to 0.01 or lower does not noticeably affect the distribution $W(n, N_0)$ in Equation (S8) and the quality of fitting in Figure S3. In contrast, the higher *p* values make the distribution significantly narrower resulting in a noticeable discrepancy between $W(n, N_0)$ and the simulated distributions (see dotted line in Figure S3b).

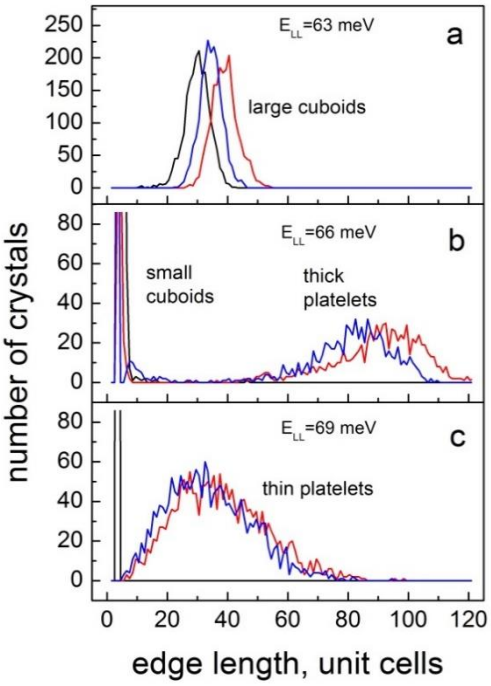

Figure S4. Distributions of short (black), medium (blue) and long (red) crystal edges in an ensemble of 3000 crystals for $\varepsilon_{AA} = 109\,meV$, $\varepsilon_{LA} = 171\,meV$, $n_A = n_L = 2.5 \cdot 10^{-4}$, $T = 134^o\,C$ and different values of ε_{LL}. a) $\varepsilon_{LL} = 63\,meV$, crystals grow as cuboids (see text for explanation), b) $\varepsilon_{LL} = 66\,meV$, this is the same as the curves in Figure 3b, a mixture of small (6-10 a_0) cuboids

and thick (6-10 a_0) platelets, c) $\varepsilon_{LL} = 69 meV$, crystals grow as thin (~4 a_0) platelets with very broad lateral size distribution.

Within the same approach, we can explain the broadening of the lateral size distribution for thin platelets shown in Figure S4c. According to Figure S5 showing excess free energy for cluster formation on a narrow ($3x10\, a_0^2$) facet (panel *c*), the energy oscillates around the almost constant level. This means that the new layer formation probability

$$P_A = K_A \cdot \exp\left(-\frac{\Delta_{CA}}{k_B T}\right),\ K_A = 1 - \exp\left(-\frac{\Delta_{AA}}{k_B T}\right) \tag{S9}$$

with Δ_{AA} representing the difference in the free energy of the atomic layer covering an entire facet and that of the critical cluster, is very low. This means that for analytical description of the edge length distribution using Equation (S8) we have to take into account a weak dependence of *p* on the facet length *n* and approximate *p* as

$$p = p_0 + p_1 \cdot n \tag{S10}$$

where p_0 and p_1 are constants. Then we obtain the distribution shown in Figure S6b, which is in a good agreement with the KMC simulation results.

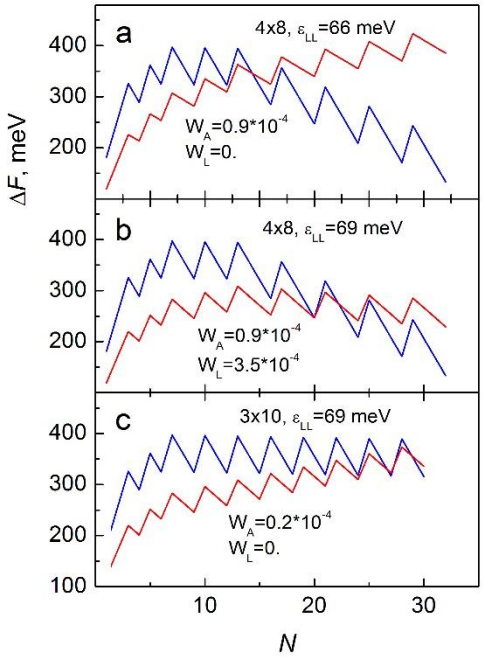

Figure S5. Excess free energies ΔF plotted versus cluster size N (given in unit cells) for different values of ε_{LL}: a) $\varepsilon_{LL} = 66\,meV$, b) and c) $\varepsilon_{LL} = 69\,meV$, and for crystal facets of different sizes: a) and b) 4x8 a_0^2 c) 3x10 a_0^2. The other parameters are $\varepsilon_{AA} = 109\,meV$, $\varepsilon_{LA} = 171\ meV$, $n_A = n_L = 2.5 \cdot 10^{-4}$, $T = 134^o\,C$. $W_{A(L)}$ is proportional to the probability of atomic (ligand) layer deposition.

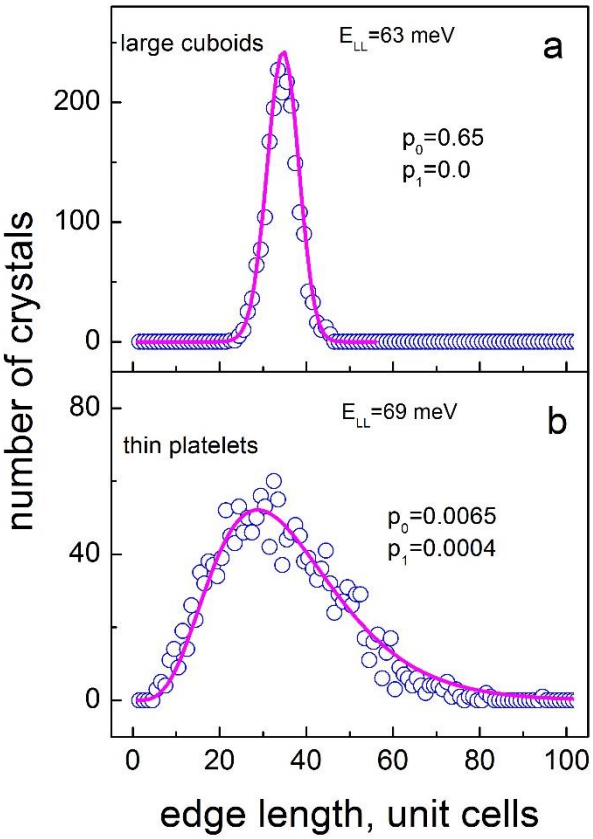

Figure S6. Medium edge length distribution obtained in KMC simulations (symbols): a) the sum of all edges distributions from Figure S4a. b) the sum of medium and long edges' distributions from Figure S4c. Solid lines are the distributions $W\left(n, N_0\right)$ for p determined by Eq. (S5).

Effects of ligand-atom interaction energy in edge size distributions

We also studied the effect of variation of the ligand-surface interaction energy ε_{LA}. The results presented in Figure S7 show that increasing ε_{LA} first decreases the NPLs thickness (panel c) and then makes the ligand cluster critical size so small that even narrow crystal facets got covered with ligand layers very quickly, which then makes any further crystal growth impossible. Decrease of ε_{LA} from 171 meV down to 169 meV results in the growing mixture of thick NPLs and nanorods (panel *b*). Further reduction of ε_{LA} down to 165 meV results in the growth of cuboid-shaped crystals. Such a tendency is understandable, as a significant decrease in ligand adhesive energy would mean no ligand is blocking layers on the crystal surfaces; hence only nano-cuboids would be able to grow.

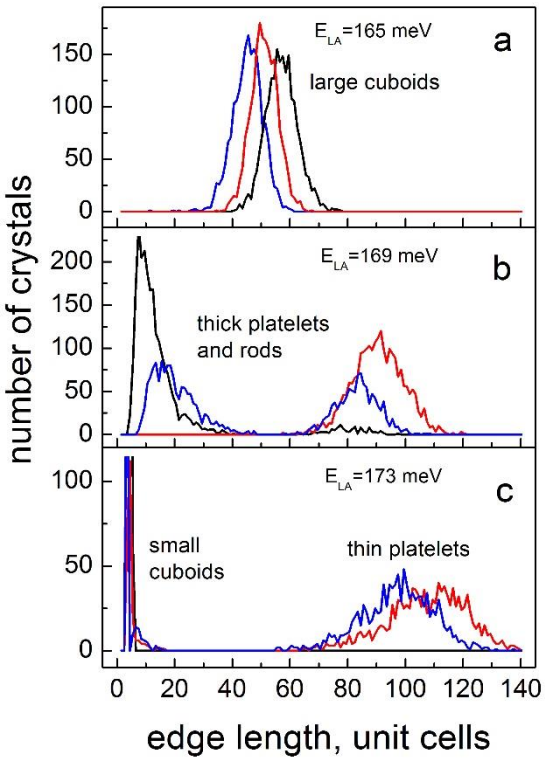

Figure S7. Distributions of short (black), medium (blue), and long (red) crystal edges in an ensemble of 3000 crystals at different ε_{LA} values for T=134 °C and initial values $n_A = n_L = 2.5 \cdot 10^{-4}$. All other energy parameters are the same as in the caption to Figure 1. a) $\varepsilon_{LA} = 165 meV$ shows the growth of cuboid-like crystals, b) $\varepsilon_{LA} = 169 meV$ indicates a mixture of thick platelets and rod-like crystals – a fraction of crystals have two edges rather short (under 30 a_0, where a_0 is the unit cell length) and one long (over 70 a_0), c) $\varepsilon_{LA} = 173 meV$ is similar to Fig. 3b is showing a mixture of small cuboids and thin NPLs.

The thicker (4 u.c.) facets are still able to grow - see Figure S2c.

EXPERIMENTAL SECTION:

All procedures were carried on a Schlenk line under oxygen-free conditions and nitrogen gas flow. **Materials.** All chemicals were used as received without further purification. Lead acetate trihydrate ($Pb(CH_3COO)_2 \cdot 3H_2O$, 99.99%), cesium carbonate (Cs_2CO_3, reagent Plus, 99%), 1-octadecene (ODE, technical grade, 90%), oleylamine (OLAM, 70%), butyric acid (≥99%), octanoic acid (≥98%), oleic acid (OA, 90%), and HBr acid (48% in water) were purchased from Sigma-Aldrich and used without further purification. All solvents such as toluene, diethyl ether, and methyl acetate were anhydrous, and the absolute ethanol were purchased from Sigma-Aldrich.

Preparation of Oleylammonium Bromide Precursor.

The reaction was performed in an ambient condition in fume hood following the procedure reported by Protesescu *et al.*[51], with modification as following. In a 500 mL flask, oleylamine (OLA, 25 mL), HBr (48% in water, 30 mL), and ethanol (100 mL, absolute >99.8%) were mixed and vigorously stirred for 4 hours at room temperature. Then the content of the flask was evaporated at 40 °C via rotary evaporation to remove all solvents. The obtained product was dissolved back in the minimum amount of absolute ethanol for the re-precipitation process to purify the product from any contamination. The solution was titrated drop by drop of diethyl ether until very few crystals start to precipitate. The flask was moved to the fridge at (–10 °C) overnight to complete the re-precipitation of pure white crystals. The white precipitate was then filtrated using Buchner filtration and placed for drying in a vacuum dryer oven at 40 °C for overnight.

Preparation of Caesium Oleate Precursor.

Synthesis of Cesium (Cs)-oleate was done according to literature.[30]

Synthesis of Caesium Lead Tribromide Perovskite Nanoplatelet.

In a typical synthesis of pristine $CsPbBr_3$ NPLs, a 2mmol of lead acetate trihydrate (76 mg) was dissolved in 1.5 mL oleic acid and 1 mL oleylamine in 5 mL of octadecene (ODE) at 120

°C, using the standard air-free technique. A previously prepared and stored under an inert atmosphere, 0.6 mL (0.125 M) of cesium oleate (preheated at 100 °C) was then injected to the solubilized lead precursor and the reaction flask left to continue stirring under vacuum at 120 °C for 1–2 hours. Then, the temperature was increased to 150 °C under the flow of N_2. In a separate vial under N_2, six mmol of oleylammonium bromide (0.21 g) was dissolved in 2 mL of anhydrous toluene and then was swiftly injected into the reaction flask at 145–150 °C. This resulted in changing the color of the reaction mixture from colorless to transparent light green (chartreuse) color, indicating the formation of the $CsPbBr_3$ NPLs. The growth of the NCs was halted after 10–20 seconds by removing the heat source, and the system was cooled with an ice-water bath while simultaneously injecting cold anhydrous toluene into the reaction mixture. The crude solution was collected into a centrifuge tube and was centrifuged for 10 min at 8000 rpm. The supernatant was collected for further use, and any precipitate was discarded.

Washing Process.

For further use or characterizations, these NCs went through a washing process. Typically, we purify the reaction crude solution by precipitating the NPLs with methyl acetate (anti-solvent) and subsequently re-dissolve in toluene to remove excess unreacted precursors. The toluene colloidal solution is added to methyl acetate in a ratio of 1 to 3. Then this mixture is centrifuged at 8000 rpm for 5 minutes to precipitate the NPs on the sidewall of the centrifuge tube. We then discard the supernatant and re-dissolve the precipitate in toluene. This washing process is repeated twice before further using of the NCs in device fabrication.

Characterization

Microstructure Characterization

Aberration-corrected scanning transmission electron microscopy (STEM) was used for the morphology characterization of the as-synthesized NPLs. Samples were deposited on standard lacey carbon grids suspended in toluene (after two cycles of washing by methyl acetate) and left in the air to dry. STEM imaging was performed on an image and probe-corrected JEOL ARM300CF, operated ta 300 kV accelerating voltage. We used a probe current of 2.2 pA for imaging (using a 20 u [micron symbol]m probe-forming aperture), providing a probe convergence semi-angle of 16.4 mrad. The annular dark-field signal was acquired at 20 cm camera length, summing the scattered electrons over the range of 36.7 and 200 mrad in semi-angle.

Size distributions of NCs on the copper grid were determined by transmission electron microscopy using a JEOL JEM–2100 TEM with a LaB6 filament operating at 200 kV for both low-magnification (TEM) and high-resolution (HRTEM) images.

UV-vis Absorption spectra were recorded using a commercial Varian Cary 60 in a 1 cm cuvette.

Steady-state PL measurement was carried out with an automated spectrofluorometer (Fluorolog, Horiba Jobin-Yvon), with a 450 W Xenon lamp excitation source and a photomultiplier tube detector. The excitation wavelength was 350 nm.

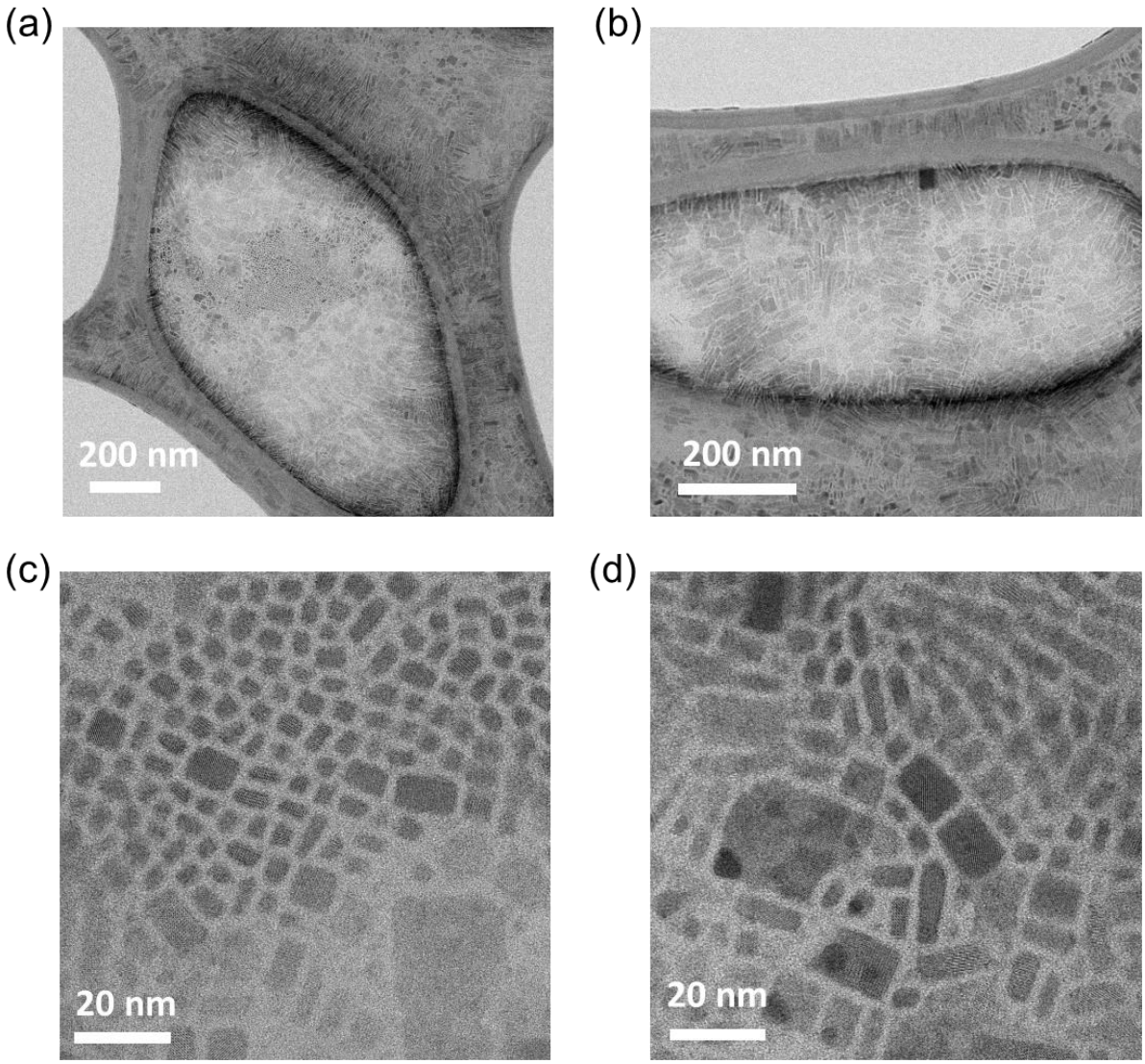

Figure S8: Low-magnification scanning transmission electron (STEM) images for $CsPbBr_3$ NCs synthesized from the three-precursor approach at 75 °C giving a mixed size of NPLs.

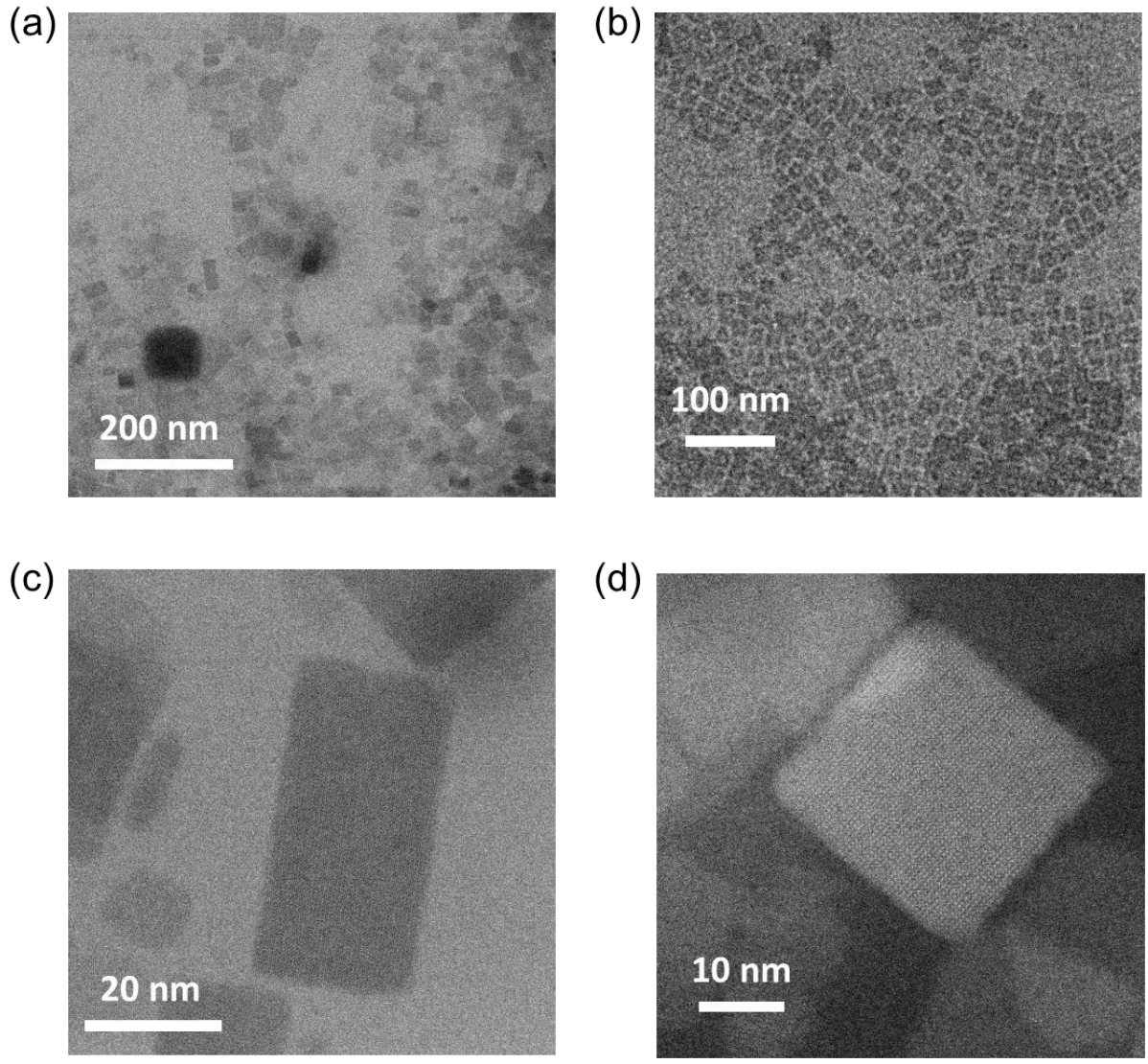

Figure S9: Low-magnification scanning transmission electron (STEM) images for $CsPbBr_3$ NCs synthesized from the three-precursor approach at 150 °C giving NPLs.

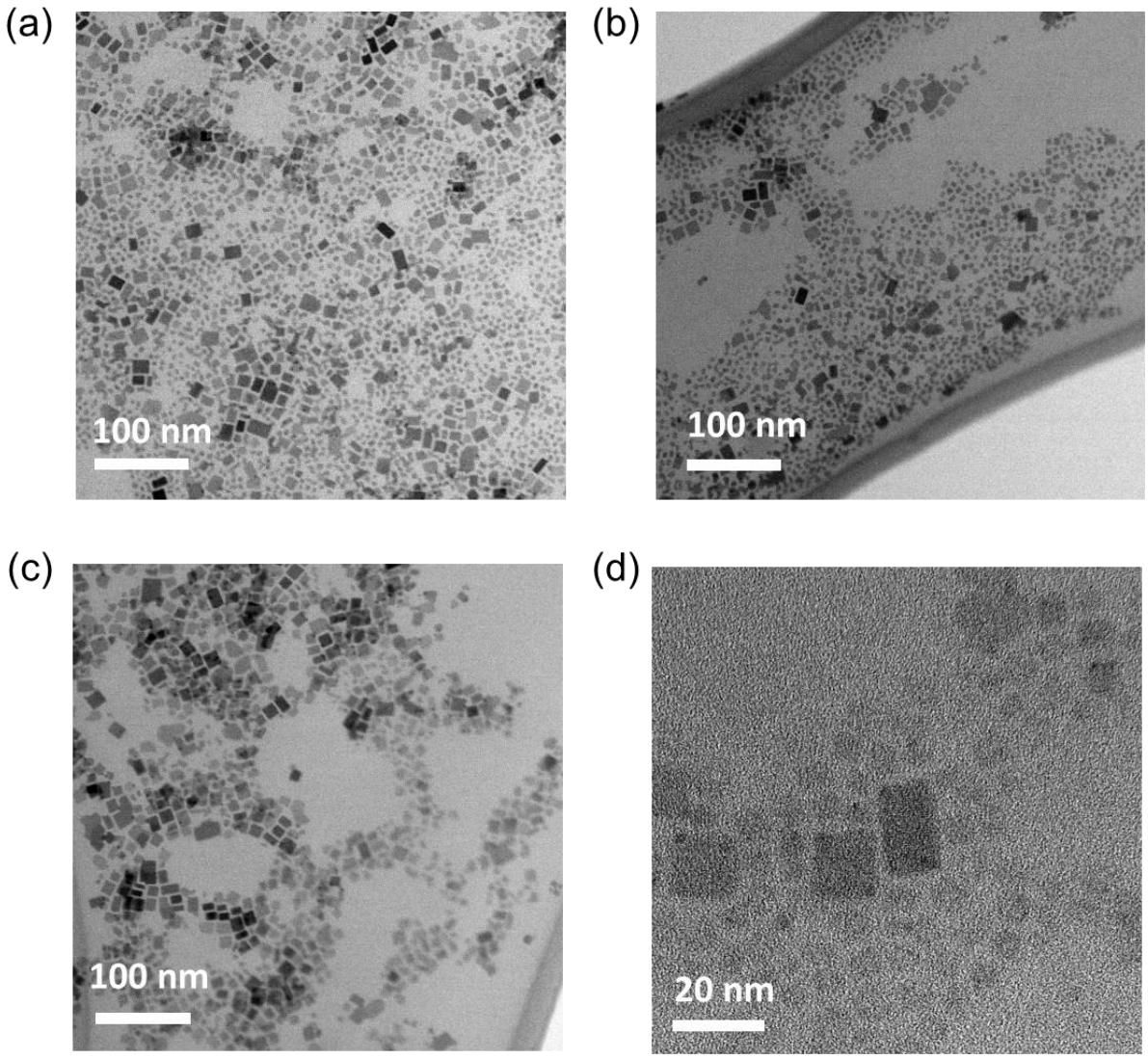

Figure S10: Low-magnification scanning transmission electron (STEM) images for $CsPbBr_3$ NCs synthesized from the three-precursor approach at 200 °C giving small cubes.

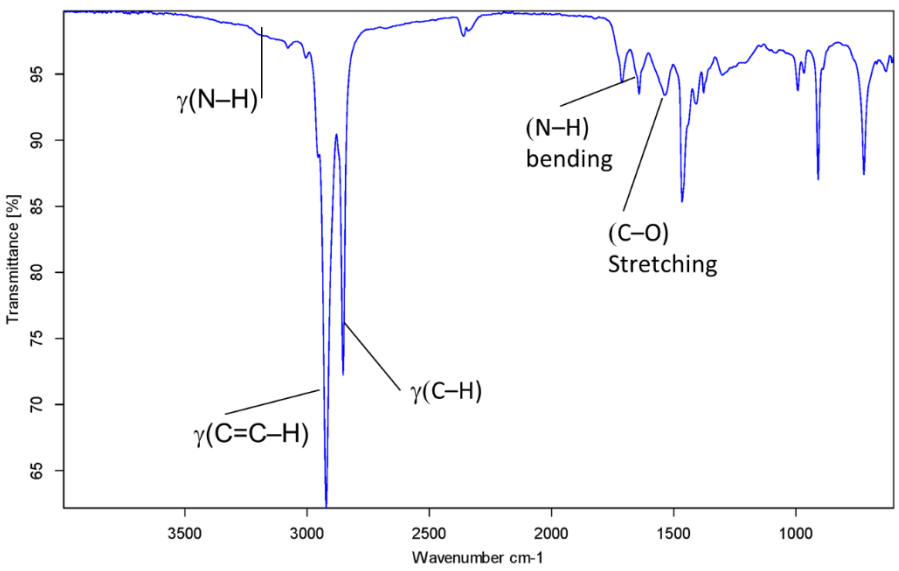

Figure S 11: Attenuated total reflection Fourier transform infrared powder spectroscopy (ATR-FTIR) of NPLs prepared at T=150 °C and in the presence of oleic acid/oleylamine mixture ligands.

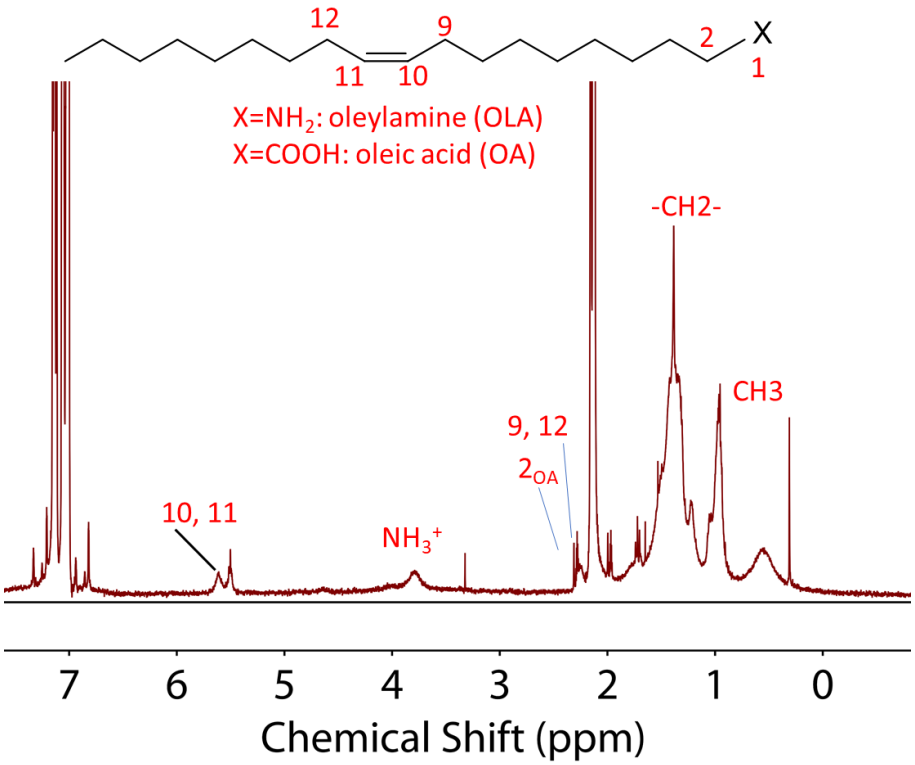

Figure S12: Proton nuclear magnetic resonance (^{1}HNMR) of NPLs prepared at T=150 °C and in the presence of oleic acid/oleylamine mixture ligands.